This is a preprint version of the paper published on *Journal of Composite Material* with the following DOI:
https://doi.org/10.1177/0021998319868293

Design and finite element assessment of Fully-Uncoupled Multi-Directional (FUMD) layups for delamination tests

Torquato Garulli[a,b], Anita Catapano[a,*], Daniele Fanteria[b], Julien Jumel[c], Eric Martin[d]

[a] *Bordeaux INP, University of Bordeaux, Laboratoire I2M CNRS UMR 5295, Talence, France*
[b] *University of Pisa, Civil and Industrial Engineering Departement, Pisa, Italy*
[c] *University of Bordeaux, Laboratoire I2M CNRS UMR 5295, Talence, France*
[d] *Bordeaux INP, University of Bordeaux, Laboratoire LCTS, CNRS UMR 5801, Talence, France*

Abstract

In this paper, a procedure to obtain *Fully-Uncoupled Multi-Directional* (FUMD) stacking sequences for delamination specimens is outlined. For such sequences, in-plane, membrane-bending and torsion-bending coupling terms are null (in closed-form solution in the framework of Classical Laminated Plate Theory, CLPT) for the entire stack and for both its halves, which form two arms in the pre-cracked region of a typical delamination specimen. This is achieved exploiting the superposition of Quasi-Trivial (QT) quasi-homogeneous stacking sequences, according to appropriate rules. Any pair of orientations of the plies embedding the delamination plane can be obtained. To assess the effectiveness of the proposed approach, a FUMD sequence is designed and compared to other relevant sequences proposed in the literature. Finite Element (FE) simulations of DCB test are performed using classic Virtual Crack Closure Technique (VCCT) and a revised state-of-the-art VCCT formulation, too. Some interesting conclusions regarding proper design of multidirectional stacks for delamination tests are drawn. Moreover, the results confirm the suitability of FUMD

*Corresponding author. Tel.: +33 55 68 45 422, Fax.: +33 54 00 06 964.
Email address: anita.catapano@bordeaux-inp.fr (Anita Catapano)

sequences for delamination tests. Thanks to their properties, these sequences might lay the foundations for the development of standard test procedures for delamination in angle-ply interfaces.

Keywords: A. Laminates, B. Fracture toughness, B. Delamination, C. Finite element analysis (FEA)

---

1. Introduction

In recent years, high performance composite materials have been more and more employed in many industrial fields, from the automotive to the aerospace. At present, even some critical primary structures are designed and realised using composites. This is due to the possibility of weight reduction that this class of materials allows. On the other hand, even if composite solutions are already in use, research on the behaviour of these structures, especially concerning the damage tolerance domain, is still ongoing. In this regard, delamination is one of the most dangerous problems for laminated composites: it is difficult to detect and leads to a drastic reduction of mechanical resistance. For these reasons, both the industry and the academy have devoted a great deal of effort to study and understand delamination [1, 2, 3, 4]. Nowadays, delamination is studied using fracture mechanics concepts [5]. Hence, according to the theory developed by Griffith [6] and Irwin [7, 8], the material parameter governing delamination is the critical value of strain Energy Release Rate (ERR). ERR is the rate of change of elastic potential energy with respect to crack advance. It is a function of geometry, material and load conditions. When ERR attains its critical value, G_c, propagation occurs.

In order to characterise delamination behaviour of composites, appropriate tests to determine the critical value of ERR have to be performed. In this regard, it's worth mentioning that some differences arise for these materials, with respect to classic homogeneous and isotropic ones. Indeed, in a body made of homogeneous isotropic material, subjected to static loads, a crack propagates following a path such that a pure opening mode at its tip is maintained [5,

9]. On the other hand, delamination is usually confined to propagate in an interlaminar layer, thus allowing the possibility to be loaded in three different modes: opening, sliding and tearing. In addition, it was shown that the critical ERR of the interface is a function of the mode mix under which delamination propagate [9]. As a consequence, characterisation of such property should be performed under the three pure modes loading conditions and under mixed mode, too. Thanks to important research efforts [10], delamination tests have been proposed, improved and eventually standardised into norms for pure mode I [11], mode II [12] and mixed mode I-II [13]. For mode III some promising tests have been proposed [14], but no standard exists yet.

However, existing standards show a critical limitation: they only apply to long fibres Uni-Directional (UD) materials with delamination fronts laying orthogonally to fibres direction. In most real applications, on the contrary, multidirectional laminates are used and delamination may appear and propagate in any interface. Consequently, since the '80s, many studies have been carried out to try and characterise fracture toughness in interfaces different from the standard $0°/0°$ one. Notwithstanding such efforts, valid fracture toughness characterisation techniques for delamination propagating at interfaces between angle plies have not been found yet.

In 2004, a comprehensive review [15] on several experimental studies conducted up to then outlined the fact that no general trend could be found to describe in a rigorous way all results, which in some cases appear to be even contrasting. A number of factors may cause the inconsistencies that these studies have brought to light. According to relevant literature and limiting the scope to mode I and mode II tests, such factors may be categorized as follows.

Additional energy dissipation mechanisms. During delamination tests on multidirectional specimens, additional damage mechanisms may be activated [16]. Indeed, off-axis plies are weak with respect to normal stresses arising during such tests and they may suffer matrix cracking. This puts into question the validity of interlaminar critical ERR calculation by standard reduction tech-

niques based on Linear Elastic Fracture Mechanics (LEFM). Moreover, crack jump phenomena were observed in End-Notched Flexure (ENF) tests in [17], and in Double Cantilever Beam (DCB) tests in [18]. In [18, 19, 20] it was observed that stiffer specimens, with stiffer arms, are less prone to matrix cracking and delamination jump.

Residual stresses. Another major concern in delamination tests is the presence of residual stresses in the specimen. In [19] it was observed that residual stresses may have an important effect on promoting matrix crack failure, and thus delamination jump. Nairn developed a theory to account for effects of such stresses in the fracture mechanics analysis of cracks in composite materials [21, 22, 23]. He found that thermal residual stresses can considerably affect interlaminar fracture toughness evaluation. Nairn's formulation was then specialised for the most common standard composite delamination tests by Yokozeki *et al.* [24]. De Morais *et al.* [25] showed, using Finite Elements (FE) analyses, that the effects of residual stresses may be reduced if sequences, even multidirectional, are chosen carefully.

Test conditions control. When performing delamination tests, control of the test conditions in terms of mode mix is mandatory: if a pure mode test is desired, contributions from other modes must be avoided; if a mixed-mode test is to be performed, the exact mode mix is to be known, in order for its results to be exploitable. While standard test procedures [11, 12, 13] address these issues for unidirectional sequences, the transferability of such practices to multidirectional ones is to be questioned, due to the presence of mechanical couplings that modify the kinematics of the specimen and that may induce parasite modes contributions. Therefore, a standard practice consists in building a FE model of the delamination test to be performed and using the Virtual Crack Closure Technique (VCCT) [26] to calculate ERR and its modal partition on the initial straight delamination front of the specimen. Thus, a qualitative assessment can be done. However, when multidirectional sequences are considered, complications arise, due to the fact that modal components of ERR, as obtained from

VCCT, may be mesh dependent [27]. As explained in [27], their computation may be a difficult task, involving a certain degree of uncertainty.

ERR distribution along delamination front. To elaborate data obtained from delamination tests, reduction techniques based on 2D theories [11] are usually adopted (a straight front and a uniform ERR distribution along it are assumed). In 1988, Davidson and Schapery [28] outlined how three dimensional effects may affect critical ERR evaluation for non-UD layups. By means of a plate analysis, they found that laminate parameter D_c, Eq. (1), is a measure of the relative difference in the deflection of the specimen arms between plane strain and plane stress conditions.

$$D_c = \frac{D_{12}^2}{D_{11} D_{22}}\,, \tag{1}$$

Terms D_{ij} are the components of the laminate stiffness matrix, obtained by Classical Laminated Plate Theory (CLPT). Thus, the higher the value of D_c, the more important three-dimensional effects become. It is also noteworthy that D_c is a measure of the bending-bending coupling of the composite laminate. For a fixed geometry, specimens with higher values of D_c show delamination fronts with higher curvature. Therefore, in [28] it is suggested that stacking sequences yielding small values of D_c be used. Such results and recommendation were confirmed in [29]. In [30, 31], parameter B_t was introduced. It is defined as:

$$B_t = \left| \frac{D_{16}}{D_{11}} \right| . \tag{2}$$

It was shown that B_t is related to asymmetry of the ERR distribution and thus skewed delamination front. Indeed, this parameter quantify bending-twisting coupling of the laminate, which clearly causes the above mentioned effects. The authors of [30, 31] insisted on the importance of finding sequences that can minimise both parameters D_c and B_t, in order to obtain correct values of critical ERR using common data reduction procedures. In 2016, Samborski [32] performed further numerical investigations on mode I delamination in multidirectional DCB specimens. His results confirmed that stacking sequence has

a major effect on critical ERR distribution along delamination front, and that differences between this distribution and that of UD specimens cannot be neglected.

In summary, a number of researches in this field have shown the importance of an appropriate design of the multidirectional stacking sequence to be used for delamination testing. In particular, the goal, as clearly explained in [33, 34], is to design a layup that could avoid additional damage mechanism, eliminate (or at least reduce) mechanical couplings, and avoid contributions to ERR due to thermal residual stresses while allowing to test any type of delamination interface (i.e. orientation of plies embedding the initial delamination plane). In this paper we focus our attention on the design of stacking sequences that can solve the problems of mechanical couplings and residual stresses.

One early layup design strategy adopted by researchers was to design sequences containing as much 0°-oriented plies as possible [17, 30] in order to lower the value of D_c. However, such sequences have arms with different stiffness and non-null membrane-bending coupling for the entire specimen. This is particularly detrimental as residual thermal stresses will be present and undesired rotations of the specimen may occur.

In recent years, quasi-trivial (QT) solutions [35] were adopted to design better stacking sequences for delamination testing. In [36], three different QT quasi-homogeneous quasi-isotropic sequences were selected and used to fabricate symmetric specimens, each arm being made of the same chosen sequence. Thus, specimen with arms of identical elastic properties were obtained. In addition, the three different sequences yielded identical stiffness matrices. This enabled to compare sequences with the same stiffness but with different plies distribution, in particular in proximity of the delamination plane. Moreover all the sequences, both for the arms and for the total specimen, show null membrane-bending coupling matrix $\mathbf{B}$ and null B_t. However, due to symmetry, only interfaces of the θ/θ type, with $\theta = 0°, 45°$ were studied. Results of the tests showed that plies next to those embedding delamination may have an effect on critical ERR values.

In [37], the same sequences and three additional ones with similar properties were used to fabricate DCB specimens. Once again, effects of the orientation of plies at the delamination interface and of the adjacent ones were observed both in initiation and propagation phases of delamination. QT solutions were used also in [38]: two QT quasi-homogeneous sequences with angle-ply orientations were chosen. Each sequence was used to fabricate symmetric and anti-symmetric DCB specimens. These specimens have: null matrix $\mathbf{B}$ and orthotropic matrices $\mathbf{A}$ and $\mathbf{D}$ for the arms and the complete sequence. However some limits still exist: neither $0^\circ/\theta$ interface type nor low values of D_c can be obtained.

Concluding, an optimal stacking sequence allowing for delamination test of possibly any type of interface and in which coupling effects are eliminated is yet to be found.

In this paper, by means of a novel approach, we obtain a special class of multidirectional stacking sequences for delamination tests. QT quasi-homogenous solutions found in [39, 40] are utilised for both specimen arms. Additionally, these sequences are carefully chosen to have exactly the same elastic properties and to comply to superposition rules presented in [39]. Thus, also the global sequence resulting from the superposition of the two arms is a QT quasi-homogeneous one. The stacks obtained have null membrane-bending coupling matrix $\mathbf{B}$ and null B_t for both arms and for the total sequence. In addition, the proposed approach allows to solve any issue related to thermal residual stresses. A special and advantageous feature of this approach is that the sequences characterising each arm can be different and thus allow to obtain any desired delamination interface. These are labelled as *Fully Uncoupled Multi-Directional* (FUMD) sequences. They might be a key tool to design multidirectional specimens for fracture toughness tests of angle-ply interfaces.

The paper is organised as follows: firstly, a brief outline of the VCCT and of the concept of QT solutions for uncoupled and/or homogeneous laminates are presented, followed by the procedure to obtain FUMD sequences. To assess the proposed approach, a FUMD sequence is compared with other sequences taken from relevant literature in terms of elastic properties. Then, FE models of the

DCB test are developed using all the sequences previously considered. ERR distributions along the initial delamination front, obtained by means of classic and revised VCCT, are compared for all the analyses. Eventually, a discussion on how the FUMD sequence compare to the others and conclusions end the paper.

2. Fundamentals of VCCT

2.1. Classic VCCT

The Virtual Crack Closure Technique is a numerical implementation of Irwin's crack closure integral [8]. It was firstly presented in [41] for 2-D problems and then extended in [42] for 3-D cases. Since then, is has been widely used in fracture mechanics analysis.

Delamination in composite materials often propagates in mixed-mode conditions [5, 26]. Furthermore, a strong dependence of the experimentally determined G_c on ERR mode mixity was observed [26, 27]. As VCCT allows to explicitly separate modal components of ERR, it has been widely used to study delamination in composite materials [26]. Using VCCT, the ERR modal components can be obtained at each node of the crack tip in a FE model; for further details the reader is addressed to [26].

It should be remarked that when using VCCT to obtain ERR modal partitioning for a crack propagating between two materials with different elastic properties some problems arise. In 1959 Williams [43] derived the crack-tip stress field for bi-material interfaces and observed that the singularity at the tip of the crack has an oscillatory behaviour. Subsequently, Raju et al. [44] showed that, for bi-material interfaces, strain energy release components depend on the virtual crack increment Δa and have an oscillatory behaviour too, while the total ERR assumes a well-defined value, disregarding the chosen Δa. As a consequence, if modal partition is performed using VCCT, a dependence on the mesh size is expected. More details about this problems can be found in [5, 27]. Moreover, [27] reviews available techniques to overcome this problem.

One of these techniques consist in using an appropriate mesh size at the crack front, in order to obtain a valid ERR modal partition. More precisely, such a method suggests that a value of Δa such that $1/20 \leq \Delta a/t_{ply} \leq 1$ should be used (where t_{ply} is the basic ply thickness).

2.2. Enhanced VCCT

In [45], Valvo showed that classic VCCT modal partition may sometimes yield negative values of some ERR modal component. This clearly represent a physical inconsistency, as ERR modal components should be non-negative.

According to [45], this inconsistency is due to the lack of energetic orthogonality between the crack-tip force components used for modal contributions calculation in the standard VCCT. Hence, Valvo developed a revised VCCT formulation for 2D[45] and 3D [46] problems. Further development may be found in [47]. The modal contributions found are positive-defined quantities, hence regaining consistency with their physical meaning. Details about this new formulation are beyond the scope of this paper, but can be found in [45, 46, 47].

3. Fundamentals and properties of quasi-trivial solutions

Consider a laminated plate composed of n plies, Figure 1. Axes x and y lay on the laminate middle plane, axis z is perpendicular to this plane. The CLPT gives the constitutive relationship between generalised forces and generalised strains of the middle plane:

$$\begin{aligned} \mathbf{N} &= \mathbf{A}\boldsymbol{\epsilon}_0 + \mathbf{B}\boldsymbol{\chi} - T\mathbf{U}\,, \\ \mathbf{M} &= \mathbf{B}\boldsymbol{\epsilon}_0 + \mathbf{D}\boldsymbol{\chi} - T\mathbf{V}\,. \end{aligned} \tag{3}$$

[Figure 1 about here.]

In Eq. (3), $\mathbf{N}$, $\mathbf{M}$, $\boldsymbol{\epsilon}_0$ and $\boldsymbol{\chi}$ are the vectors of in-plane resultant forces and bending moments per unit length, in-plane strains and curvatures of the middle plane of the laminate, respectively; T is the actual temperature, evaluated with respect to that of the reference unstrained condition, which is, for laminates,

the curing temperature. $\mathbf{A}$, $\mathbf{B}$ and $\mathbf{D}$ are the membrane, membrane/bending coupling and bending stiffness matrices, respectively; matrices $\mathbf{U}$ and $\mathbf{V}$ express in-plane forces and moments caused by thermal effects, respectively. For a laminate with identical plies (i.e. made of the same material and having the same thickness) the following relationships hold:

$$\mathbf{A} = \frac{h}{n}\sum_{k=1}^{n}\mathbf{Q}(\delta_k)\,, \quad \mathbf{B} = \frac{1}{2}\frac{h^2}{n^2}\sum_{k=1}^{n}b_k\mathbf{Q}(\delta_k)\,, \quad \mathbf{D} = \frac{1}{12}\frac{h^3}{n^3}\sum_{k=1}^{n}d_k\mathbf{Q}(\delta_k)\,, \tag{4}$$

$$\mathbf{U} = \frac{h}{n}\sum_{k=1}^{n}\mathbf{Q}(\delta_k)\boldsymbol{\alpha}(\delta_k)\,, \quad \mathbf{V} = \frac{1}{2}\frac{h^2}{n^2}\sum_{k=1}^{n}b_k\mathbf{Q}(\delta_k)\boldsymbol{\alpha}(\delta_k)\,. \tag{5}$$

In Eq. (4), δ_k is the orientation angle of the k-th ply, $\mathbf{Q}(\delta_k)$ is its reduced stiffness matrix and $\boldsymbol{\alpha}(\delta_k)$ is its vector of thermal expansion coefficients. Coefficients b_k and d_k depend on the position k of the ply within the stack:

$$b_k = 2k - n - 1\,, \tag{6}$$

$$d_k = 12k(k-n-1) + 4 + 3n(n+2)\,. \tag{7}$$

For convenience, normalised stiffness matrices are defined as follows:

$$\begin{gathered}\mathbf{A}^* = \tfrac{\mathbf{A}}{h}, \qquad \mathbf{B}^* = 2\tfrac{\mathbf{B}}{h^2}, \qquad \mathbf{D}^* = 12\tfrac{\mathbf{D}}{h^3}, \\ \mathbf{U}^* = \tfrac{\mathbf{U}}{h}, \qquad \mathbf{V}^* = 2\tfrac{\mathbf{V}}{h^2}.\end{gathered} \tag{8}$$

In addition, the laminate homogeneity matrix is defined as:

$$\mathbf{C} = \mathbf{A}^* - \mathbf{D}^*\,; \tag{9}$$

it measures the differences between normalised membrane and bending behaviours.

A laminate is said to be *uncoupled* if:

$$\mathbf{B} = \mathbf{0}\,, \tag{10}$$

while it is said *homogeneous* if:

$$\mathbf{C} = \mathbf{0}\,. \tag{11}$$

Eventually, a laminate is *quasi-homogeneous* if properties (10) and (11) hold simultaneously.

Vannucci and Verchery [35] used the polar formalism to represent matrices $\mathbf{A}^*$, $\mathbf{B}^*$, $\mathbf{D}^*$ and $\mathbf{C}$ and to rewrite Eqs. (10) as:

$$\sum_{k=1}^{n} b_k e^{4i\delta_k} = 0, \quad \sum_{k=1}^{n} b_k e^{2i\delta_k} = 0, \tag{12}$$

to satisfy uncoupling, and (11) as:

$$\sum_{k=1}^{n} c_k e^{4i\delta_k} = 0, \quad \sum_{k=1}^{n} c_k e^{2i\delta_k} = 0, \tag{13}$$

to satisfy homogeneity. In Eq. (13), c_k is a coefficient related to matrix $\mathbf{C}$ that can be written as:

$$c_k = -2n^2 - 12k(k-n-1) - 4 - 6n\,. \tag{14}$$

It can be verified that coefficient b_k varies linearly with ply index k, whilst c_k is symmetric with a parabolic variation with respect to k. This is shown in Fig. 2 for the case of a laminate composed of 12 plies.

[Figure 2 about here.]

The sum of each coefficient over the interval $[1, n]$ is always null:

$$\sum_{k=1}^{n} b_k = 0, \quad \sum_{k=1}^{n} c_k = 0. \tag{15}$$

The concept of QT solutions can be explained as follows. Consider a laminate composed of n plies and m different orientation angles and let G_j be the set of indexes of those plies that share the same orientation angle θ_j, i.e.:

$$G_j = \{k : \delta_k = \theta_j\}\ . \tag{16}$$

The union of the m sets associated with all the orientations gives the complete set of ply indexes of the laminate, $k = 1, ..., n$. Expressions in Eqs. (12) and (13) can be split as sums over the different sets G_j, $j = 1, ..., m$:

$$\sum_{k=1}^{n} b_k e^{4i\delta_k} = \sum_{j=1}^{m} e^{4i\theta_j} \sum_{k\in G_j} b_k\ , \qquad \sum_{k=1}^{n} b_k e^{2i\delta_k} = \sum_{j=1}^{m} e^{2i\theta_j} \sum_{k\in G_j} b_k\ , \tag{17}$$

$$\sum_{k=1}^{n} c_k e^{4i\delta_k} = \sum_{j=1}^{m} e^{4i\theta_j} \sum_{k\in G_j} c_k\ , \qquad \sum_{k=1}^{n} c_k e^{2i\delta_k} = \sum_{j=1}^{m} e^{2i\theta_j} \sum_{k\in G_j} c_k\ . \tag{18}$$

Therefore, if the sum of coefficients b_k or c_k is null over each set G_j, then uncoupling or homogeneity requirements are satisfied, regardless of the values assumed by θ_j. Indeed, only the ply position in the stack will be crucial to meet these requirements. In this context, a group of plies oriented at θ_j, for which:

$$\sum_{k \in G_j} b_k = 0, \quad j = 1, ..., m\,, \tag{19}$$

$$\sum_{k \in G_j} c_k = 0, \quad j = 1, ..., m\,, \tag{20}$$

is called *saturated group* with respect to coefficients b_k or c_k, respectively; the related set of indexes G_j is called *saturated set*. A QT stack is entirely composed of saturated groups.

Since a QT stack can satisfy uncoupling, homogeneity or quasi-homogeneity conditions regardless to the value of the orientation angle characterising each saturated group, the orientation angles can be chosen/optimised to satisfy further requirements (elastic properties along some prescribed directions, buckling behaviour, natural frequencies, etc.).

From a thermo-mechanical standpoint, it is clear from Eq. (5) that if a sequence is QT uncoupled, then also matrix $\mathbf{V}$ is identically null for that sequence [35].

4. Fully Uncoupled Multi-Directional (FUMD) delamination specimen design

We define a multidirectional stacking sequence (or laminate) for delamination tests as *Fully Uncoupled Multi-Directional* if it meets the following requirements:

1. possibility to have different types of delamination interfaces;
2. avoidance of thermal residual stresses effects on ERR;
3. membrane-bending uncoupling, i.e. $\mathbf{B}$=$\mathbf{0}$;
4. in-plane uncoupling, i.e. $A_{16} = A_{26} = 0$;
5. bending-torsion uncoupling, i.e. $D_{16} = D_{26} = 0$, and hence $B_t = 0$.

Requirements 3 to 5 must be verified by the complete laminate and the two sub-laminates constituting its arms, too. In addition, the weakest possible bending-bending coupling, i.e. D_c, is desirable.

To satisfy such requirements, superposed QT sequences are used, see [39]. The strategy proposed is composed of two consecutive steps:

1. Among QT solutions, sequences able to satisfy all requirements for each of the two arms of the specimen are searched;
2. Among the sequences found in step 1, those that superposed give a macro-sequence satisfying all the requirements are eventually chosen.

The whole procedure is detailed in the following subsections.

4.1. Specimen arms sequences search

In order to perform this first step of the design process, an algorithm has been developed in order to select sequences satisfying all of the requirements imposed to the specimen arms. Such sequences are selected from a database of QT quasi-homogeneous stacks created in framework of [39]. For these stacks $\mathbf{B}=\mathbf{0}$, $\mathbf{V}=\mathbf{0}$ and $\mathbf{A}^*=\mathbf{D}^*$. Since, in general, in-plane and bending-torsion couplings are not null, only sequences allowing to obtain orthotropic matrix $\mathbf{A}$ and, by virtue of quasi-homogeneity (Eq. (11)), orthotropic matrix $\mathbf{D}$, are selected. Orthotropy of matrix $\mathbf{A}$ may be obtained, for example, using an angle-ply lamination, i.e. a sequence in which for each ply at any orientation θ, another ply at orientation -θ exists. Therefore, among QT quasi-homogeneous sequences, all those having two saturated groups with the same number of plies are selected. It is easy to verify from Eq. (5) that, as a consequence, the third component of $\mathbf{U}$ is identically null.

In addition, a third orientation group in the sequences would be desirable, in order to use also 0° oriented plies: this allows $0°/\theta$ interfaces and contributes to lower D_c (a similar effect would be obtained using 90° oriented plies, but these latter would made the specimen more compliant, which should be avoided, see Sect. 1). Furthermore, having such plies in the sequence neither affects the

already established orthotropy of the laminate (as 0° is a direction of orthotropy) nor modifies the third component of $\mathbf{U}$ which remains identically null (as 0° oriented plies do not contribute to this term). Therefore, among all usable sequences, those with three groups have been chosen. It is to be remarked that also solutions with more orientation groups may be reduced to have 3 orientation groups [39] and thus be used. This complicates the search, but leads to a significantly higher number of viable sequences.

4.2. Complete sequence construction

Once sequences for the two arms of the specimen have been selected, it is necessary to pick those that, once superposed, give a FUMD sequence. Once again, main results from [39] are exploited. Indeed, through the use of the appropriate rule, it is possible to superpose QT quasi-homogeneous sequences that result in a new QT quasi-homogeneous one. In [39] it has been demonstrated that the main rule to ensure the quasi-homogeneity of a stack obtained as superposition of two QT quasi-homogeneous elementary stacks is:

$$(n_1 n_{G_j^{(2)}} - n_2 n_{G_j^{(1)}}) = 0, \quad j = 1, ..., m^* \,. \tag{21}$$

where n_i and $n_{G_j^{(i)}}$ $(i = 1, 2)$ are respectively the total number of plies and the number of plies belonging to the j-th orientation group of the i-th sequence. Eq. (21) is specialised for the present case, where $n_1 = n_2$ and three orientation groups are used:

$$n_{G_j^{(2)}} = n_{G_j^{(1)}}, \quad j = 1, ..., 3 \,. \tag{22}$$

In other words, it is sufficient that the two superposed sequences have the same number of plies for each orientation group: this is an extremely easy condition to be met, due to the very particular case considered. We remark here that, as a consequence of Eq. (22), $\mathbf{A}$, $\mathbf{D}$ and $\mathbf{U}$ will be identical for the two specimen arms.

If the complete sequence is a QT quasi-homogeneous one, Eq. (10) stands: no membrane-bending coupling is exists and also $\mathbf{V} = \mathbf{0}$. Moreover, as the two

sub-laminates have an angle-ply lamination sequence, the macro-stack will have an angle ply lamination too, with the already chosen orientations and with the same percentages of plies per orientation as the arms. Therefore, as Eq. (11) stands too, the complete sequence will have orthotropic matrices $\mathbf{A}$ and $\mathbf{D}$, as required. In addition:

- the complete sequence and both arms have identical $\mathbf{A}^*$, $\mathbf{B}^*$, $\mathbf{D}^*$, $\mathbf{U}^*$ and $\mathbf{V}^*$. Moreover, $\mathbf{B} = \mathbf{0}$ and $\mathbf{V} = \mathbf{0}$, and the third component of $\mathbf{U}$ is identically null too. This leads to: first, the three parts of the specimen have identical Coefficients of Thermal Expansion(CTEs); second, only extensional CTEs are non-null (in-plane shear CTE is null, and bending CTEs are null). This eventually means that no residual stresses effect on ERR will exists [22, 24]. More details about CTEs computation may be found in Appendix A;
- if a great number of 0° oriented plies is present in each arm, the same is valid for the complete sequence; bending-bending coupling, then, will be weak for the complete specimen too;
- through this strategy, a lot of FUMD sequences may be generated, allowing for different interface types and orientations.

In order to show the effectiveness of FUMD sequences, one such sequence with a total of 28 plies and labelled *'QT'* has been developed and will be compared, in the following sections, to other sequences proposed in the literature to serve the same scope, i.e. delamination testing. Plies orientations used for sequence *'QT'* are ±45° and 0°. While these can be chosen freely without affecting the quasi-triviality of the stack, this choice allows to obtain a 0°/45° delamination interface, very common in practical applications.

For the comparison, sequences conceived for pure mode I DCB tests and that share the same delamination interface, 0°/45°, have been chosen. They are reported in Table 1. The interested reader will find other interesting sequences, for different delamination tests, in references [33] and [34].

In order to show the effectiveness of the approach, a FUMD sequence of 28

plies has been designed and is reported in Table 1, under the label *'QT'*. For this particular study, plies orientations used for sequence *'QT'* are $\pm 45°$ and $0°$, and a $0°/45°$ delamination interface is studied. Two reasons dictate this choice: first, such interface is very common in practical applications, and second, existing literature offers a solid ground to evaluate the proposed approach for this particular case. Indeed, sequence *'QT'* will be compared, in the following sections, to other ones proposed in the literature and conceived for pure mode I DCB tests. All such sequences share the same delamination interface, $0°/45°$. They are reported in Table 1. However since orientations for FUMD sequences can be arbitrarily chosen, the approach is valid to design delamination specimens having any desired delamination interface. Other examples of interesting sequences, for different delamination tests, can be found in references [33] and [34].

[Table 1 about here.]

Clearly, the elastic properties of the compared sequences are different and depend on the stacking sequence. As a reference, therefore, the D_{11}^* terms for each sequence and both its arms are reported in Table 1. The UD sequence (the only one allowed by the ASTM standard [11]) is presented as the ideal reference.

[Table 2 about here.]

All sequences in Table 1 have been conceived with the aim of minimising coupling effects, in order to be suitable for delamination testing.

Tables 2-4 show a synthesis of the elastic characteristics obtained for each sequence, as computed using CLPT. More precisely, Table 2 is relative to the lower arm sequence, Table 3 to the upper arm sequence and Table 4 to the complete sequence. Indices *up* and *down* are used to refer to quantities computed for the upper arm and the lower arm of the specimen, respectively.

[Table 3 about here.]

On top of D_c and B_t parameters, Tables 2-4 shows the achievements in terms of membrane-bending uncoupling, homogeneity and equality of stiffness matrices

between upper arm and lower arm sequences. These differences may be relevant as they quantify stiffness asymmetry in the specimen, which may lead to parasite modes contributions during delamination tests.

It can be seen from Tables 2-4 that sequence QT yields slightly higher values, with respect to some other sequence, for the D_c parameter, reason why a more curved mode I ERR distribution may be expected. However it appears clear how sequence QT is the one that best reproduces the elastic properties of the ideal UD sequence.

[Table 4 about here.]

5. Assessment of the approach via Finite Element (FE) analyses

A standard practice to qualitatively assess the suitability of multidirectional stacking sequences for delamination tests [19, 25, 32, 38, 48] is the use of crack closure techniques (in particular the Virtual Crack Closure Technique, VCCT) to evaluate ERR distribution at the initial straight delamination front. Thus, effects of layup can be observed and sequences achieving the best (i.e. the most symmetric and flat) distributions can be chosen and used for experimental testing. In addition, modes contributions can be estimated too: if a pure mode delamination test is to be performed, it is desirable to have the weakest possible contributions from non-concerned modes.

Hence, in compliance with this approach, a FE model of the DCB test has been developed. To perform ERR computation, firstly the classical VCCT formulation [26] has been used. Then, an enhanced recent VCCT formulation [45] has been used to double check results. A comparison between the two techniques will be laid out.

The DCB FE model is built using the commercial FE software Abaqus, and is shown in Fig. 3. The relevant dimensions of the model are: length (l) 150 mm, width (b) 25 mm and initial delamination length (a_0) 50 mm. The material is a carbon/epoxy composite, with ply thickness of 0.125 mm, whose properties are listed in Table 5.

[Figure 3 about here.]

[Table 5 about here.]

The region across the delamination front is modelled using fully-integrated 3D brick elements (C3D8) and a ply-by-ply refinement, i.e. each ply is represented with an element through the thickness. The material orientation of each layer is assigned according to the orientation of the corresponding ply. The regions far from the delamination front are modelled as separated part objects and attached to the central refined part by means of tie constraints. Continuum shell elements (SC8R) are used to model these regions and the number of elements through the thickness is automatically adjusted, based on the total number of plies in the sequence and on the desired number of plies within each element.

Eight mesh transitions are introduced to obtain the desired mesh size and their locations may be defined by the user. These transitions are script-generated in order to guarantee mesh continuity, thus avoiding the necessity of defining multiple parts and constraints and allowing to obtain a mesh using no other elements than hexaedral ones. This allows to obtain an extreme refinement in the vicinity of the front and a coarser mesh in the farther regions, while having the smoothest transition possible. Thus, great accuracy is achieved at crack front, while computational costs remain affordable.

To simulate a DCB test, a dynamic step accounting for geometric non-linearities is performed and the implicit solver of the software is used. The opening displacement is assigned to two reference nodes that are linked to the nodes of the relevant edges of the specimen by means of multi-point-constraints (MPC). In the vicinity of the crack front, along the insert interface, contact between the two arms of the specimen is modelled using a hard contact pressure-overclosure relationship with direct enforcement method, i.e. no interpenetration at all is allowed between the specimen arms.

In these analyses, thermal effects are not simulated. It's noteworthy, however, that sequence QT is the only one that is expected not to be affected by

thermal residual stresses, thanks to the already discussed properties of its CTEs. More details and the numerical computation of CTEs for all the sequences of Table 1 may be found in Appendix A.

A preliminary study has been performed to chose an appropriate crack-tip mesh size. Different mesh sizes giving $\Delta a/t_{ply}$ ratios falling in the interval $[0.4, 1]$ have been used. Results were fairly stable and eventually a crack-tip mesh size of 0.0781 mm has been chosen as a good compromise between computational cost and accuracy.

6. Results and discussion

6.1. FE simulation results: classic VCCT

Using VCCT, the ERR distributions at the straight crack front as well as the overall modal contributions have been determined for all sequences listed in Table 1. Figs. 4-6 show respectively the mode I, II and III ERR distributions along the crack front, normalised by the average total ERR of the respective sequence.

[Figure 4 about here.]

In Fig. 4, concerning mode I distributions, sequences can be grouped into two sets based on their behaviour:

1. ERR distributions of sequences QT and DeM_B, which are more curved, and reach a higher peak. On the other hand these distributions seem fairly symmetrical, the QT one being more symmetrical than the other one;
2. ERR distributions of other sequences, which are flatter but seem more asymmetrical.

This behaviour is readily explained: the first two sequences have a significantly lower number of 0° oriented plies with respect to the other ones. This translates in a stronger bending-bending coupling (thus higher D_c value), which makes mode I ERR distribution more curved. It's noteworthy that choosing longer

FUMD sequences (thus allowing a reduction of the parameter D_c) this aspect can be improved. Of course, the curve from the UD sequence stands as the ideal one: symmetrical and quite flat in the middle part.

[Figure 5 about here.]

[Figure 6 about here.]

[Figure 7 about here.]

On the other hand, by plotting mode II and III ERR distributions, in Figs. 5 and 6 respectively, more interesting results emerge. As expected, the UD sequence has identically null distributions for both modes. Remarkably, however, sequence QT is the one yielding the lowest contributions of mode II and III, with distributions that approach more closely those of UD sequence. Also, Fig. 5 shows that significant mode II contribution may be present along the whole delamination front(even in the middle of the specimen), if the stacking sequence is not carefully designed. This is clearly reflected in Fig. 7 too, where the overall (i.e. considering the entire crack front) percent contributes of mode II and III ERR with respect to the total ERR are shown. As it can be seen, QT sequence is the one yielding the best results, with a significant difference with respect to the other sequences.

These results, albeit qualitative, show clearly the potential of FUMD sequences for delamination testing.

6.2. FE simulation results: revised VCCT

Fig. 6 highlights that negative values of mode III ERR may be found. This rise doubts on the validity of the modal partition performed using standard VCCT, so analyses were performed using the revised VCCT formulation proposed in [45]. To the best of the authors knowledge it's the first time this technique is implemented in a 3D FE model.

[Figure 8 about here.]

[Figure 9 about here.]

[Figure 10 about here.]

[Figure 11 about here.]

The results obtained using revised VCCT are plotted in Figs. 8-10, which show mode I, II and III ERR distributions, normalised by the average value of the total ERR.

Concerning mode I ERR distributions, Fig. 8, no significant differcences are observed when comparing revised VCCT results to those obtained using the classic VCCT. On the other hand, for mode II and III distributions, Figs. 9 and 10 respectively, some slight differences may be observed. In particular, mode III distributions are generally lower than those obtained with classic VCCT. This can be clearly observed at the left (negative y) edge of the specimen, where peak values are about one half of those obtained with standard VCCT. As expected, no negative values are obtained this time. Fig. 11 confirms the qualitative trend observed in Fig 7. However, it is noteworthy that mode III contributions are reduced in favour of mode II ones.

While conclusions based on standard VCCT data on the quality of the FUMD specimen are confirmed by the revised VCCT, some differences may arise in the evaluation of local effects on mode II and mode III ERR distributions. It is possible, therefore, that the standard VCCT formulation may not be adequate and might yield unsatisfying results for particular cases where localized effects (such as edge effects) are of interest. Hence, caution is advised when interpreting results obtained by means of classic VCCT analyses.

[Figure 12 about here.]

For this reason, further analyses have been performed using the revised VCCT formulation.

Figs. 12-14 show previous data using a different normalisation, as in [25]: the local percent contribution of each mode to the local value of total ERR is

plotted along the delamination front[1].

Therefore, these figures show at any point of the delamination front the contribute of each mode to the total local ERR. Fig. 12 shows that sequence QT is the one that guarantees the highest and widest dominance of mode I over the specimen width, reaching even the edges of the specimen. On the other hand, other sequences show a steep decrease in mode I dominance when approaching the edges of the specimen, where modes II and III become dominant, as confirmed by Figs. 13 and 14.

[Figure 13 about here.]

[Figure 14 about here.]

Results presented above can be analysed by means of performance indexes reported in Table 6. They are:

1. the overall modes II and III ERR percent contributes (G_2 % and G_3 %, respectively). Low values of such parameters should be obtained since, for a sound characterisation of pure modes delamination fracture toughness, all contributes from undesired modes should be eliminated. Data show that sequence QT is able to keep these parameters much lower than the other sequences;
2. a parameter quantifying curvature of mode I ERR distribution (β) defined as:
$$\beta = \frac{G_1^{max} - G_1^{av}}{G_1^{av}}\,, \tag{23}$$
and already used in previous studies on the topic [38, 48]. It can be seen that sequences QT and DeM_B show slightly higher values of this parameter compared to other ones and in accordance with their higher values of D_c. In [38] it was shown how to effectively take into account the curvature of mode I ERR distribution by using β in the experimental critical ERR evaluation;

[1]The value at each point is obtained dividing $G_i(y)$ $(i = 1, 2, 3)$ by the value of $G_{tot}(y)$.

3. a parameter (γ) that quantifies the asymmetry of the distribution of mode I ERR. It evaluates the difference of G_1 normalised value between each couple nodes on the delamination front that are positioned symmetrically with respect to the specimen longitudinal geometrical symmetry plane:

$$\gamma = \sqrt{\frac{\sum_{n^{(+)}} \left(\frac{G_1(y) - G_1(-y)}{G_1^{av}}\right)^2}{n_{nodes}/2}}, \tag{24}$$

where n_{nodes} is the number of nodes along the delamination front and $n^{(+)}$ is the subset of such nodes that have a positive y coordinate. The asymmetry of the ERR distribution may invalidate data reduction procedures. For the ideal UD sequence there is no asymmetry. On the other hand, concerning the multidirectional stacks analysed, sequence QT is the one showing the lowest value, as reported in Table 6.

[Table 6 about here.]

The values of the parameters in Table 6 should be as low as possible in order to obtain optimal test conditions. Indeed, this is evident observing values obtained for the UD sequence, which is, of course, the one that best meets all requirements. Moreover, comparing Tables 2-4 to Table 6 it can be seen that, apparently, some correlations may exist between the elastic properties of the stacks and the ERR that they produce, beyond the commonly assumed indicators D_c and B_t. Further activities to better analyse this aspect are needed.

7. Conclusions

In this paper, a procedure to design a *Fully-Uncoupled Multi-Directional* specimen for delamination tests was described. The procedure exploits a particular class of stacking sequences (quasi-trivial ones) and recently derived criteria for the superposition of these stacks that allow to obtain new QT stacks.

The proposed approach addresses and solves many problems, identified by decades of research, concerning the design of sequences for delamination testing of non $0°/0°$ interfaces: it eliminates all mechanical couplings, it avoids

effects of thermal residual stresses and it also allows for testing a wide variety of delamination interfaces.

While any delamination interface can be obtained by using the proposed approach, a delamination specimen having a $0°/45°$ delamination interface has been designed using a FUMD sequence; this choice allowed to compare such laminate to others having the same interface and proposed in the literature for the same purpose.

It has been shown that, from an elastic point of view, the behaviour of the proposed sequence is the closest to that of an UD stacking sequence. Then, FE analyses have been performed and ERR mode partitioning has been evaluated using classical VCCT and a revised formulation, that shows a physically consistent ERR modal partition. Indeed, the appearance of negative values of ERR, occurring using classical VCCT, is thus avoided.

The numerical results obtained show that the FUMD sequences are those that reduce parasite modes contribution the most, when performing Mode I standard delamination tests on multi-directional interfaces, if compared to other sequences designed for the same purpose.

For all these reasons, the proposed approach may represents a tangible step toward the creation of standardised tests for delamination in multi-directional interfaces.

Acknowledgements

The first author is grateful to region Nouvelle-Aquitaine for supporting this research work through the SMARTCOMPOSITE project.

Appendix A. Laminate equivalent Coefficients of Thermal Expansion

This appendix shows the procedure to obtain effective (or apparent) CTEs in the framework of CLPT. The interested reader may found more details in Refs. [9] and [49].

Eq.(3), from CLPT, may be written in matrix form, as follows:

$$\begin{Bmatrix} \mathbf{N} \\ \mathbf{M} \end{Bmatrix} = \begin{bmatrix} \mathbf{A} & \mathbf{B} \\ \mathbf{B} & \mathbf{D} \end{bmatrix} \begin{Bmatrix} \boldsymbol{\epsilon}^0 \\ \boldsymbol{\chi} \end{Bmatrix} - T \begin{Bmatrix} \mathbf{U} \\ \mathbf{V} \end{Bmatrix}, \tag{A.1}$$

where all terms have been defined in Section 3. By additionally defining:

$$\begin{Bmatrix} \mathbf{N}^* \\ \mathbf{M}^* \end{Bmatrix} = T \begin{Bmatrix} \mathbf{U} \\ \mathbf{V} \end{Bmatrix}, \tag{A.2}$$

we can rewrite Eq. (A.1) as:

$$\begin{Bmatrix} \mathbf{N} + \mathbf{N}^* \\ \mathbf{M} + \mathbf{M}^* \end{Bmatrix} = \begin{bmatrix} \mathbf{A} & \mathbf{B} \\ \mathbf{B} & \mathbf{D} \end{bmatrix} \begin{Bmatrix} \boldsymbol{\epsilon}^0 \\ \boldsymbol{\chi} \end{Bmatrix}. \tag{A.3}$$

Eq. (A.3) may be inverted to obtain:

$$\begin{Bmatrix} \boldsymbol{\epsilon}^0 \\ \boldsymbol{\chi} \end{Bmatrix} = \begin{bmatrix} \mathbf{a} & \mathbf{b} \\ \mathbf{b}^T & \mathbf{d} \end{bmatrix} \begin{Bmatrix} \mathbf{N} + \mathbf{N}^* \\ \mathbf{M} + \mathbf{M}^* \end{Bmatrix}, \tag{A.4}$$

where

$$\begin{bmatrix} \mathbf{A} & \mathbf{B} \\ \mathbf{B} & \mathbf{D} \end{bmatrix}^{-1} = \begin{bmatrix} \mathbf{a} & \mathbf{b} \\ \mathbf{b}^T & \mathbf{d} \end{bmatrix}, \tag{A.5}$$

$$\mathbf{a} = (\mathbf{A} - \mathbf{B}\mathbf{D}^{-1}\mathbf{B})^{-1}, \tag{A.6}$$

$$\mathbf{b} = -\mathbf{a}\mathbf{B}\mathbf{D}^{-1}, \tag{A.7}$$

$$\mathbf{d} = (\mathbf{D} - \mathbf{B}\mathbf{A}^{-1}\mathbf{B})^{-1}. \tag{A.8}$$

Substituting Eq. (A.2) into Eq. (A.4) gives:

$$\begin{Bmatrix} \boldsymbol{\epsilon}^0 \\ \boldsymbol{\chi} \end{Bmatrix} = \begin{bmatrix} \mathbf{a} & \mathbf{b} \\ \mathbf{b}^T & \mathbf{d} \end{bmatrix} \begin{Bmatrix} \mathbf{N} \\ \mathbf{M} \end{Bmatrix} + T \begin{Bmatrix} \boldsymbol{\alpha}_\epsilon \\ \boldsymbol{\alpha}_\chi \end{Bmatrix}. \tag{A.9}$$

In Eq. (A.9), $\boldsymbol{\alpha}_\epsilon$ and $\boldsymbol{\alpha}_\chi$ are the vectors of in-plane and bending effective laminate CTEs, respecctively. They are obtained as:

$$\begin{Bmatrix} \boldsymbol{\alpha}_\epsilon \\ \boldsymbol{\alpha}_\chi \end{Bmatrix} = \begin{bmatrix} \mathbf{a} & \mathbf{b} \\ \mathbf{b}^T & \mathbf{d} \end{bmatrix} \begin{Bmatrix} \mathbf{U} \\ \mathbf{V} \end{Bmatrix}. \tag{A.10}$$

Eq. (A.10) allows to compute the effective CTEs for any given laminates. Let us assume, for the basic ply:

$$\left\{\begin{array}{c}\alpha_1\\ \alpha_2\\ \alpha_{12}\end{array}\right\} = \left\{\begin{array}{c}-0.04 * 10^{-6}\\ 18.00 * 10^{-6}\\ 0\end{array}\right\} \quad [1/K]\,, \tag{A.11}$$

In Eq. (A.11), α_1 is the CTE along fibres direction, α_2 is that along transverse direction. These values may be representative of a carbon/epoxy UD layer. Using such values and Eq. (A.10), CTEs for the sequences compared in the paper have been computed. The results, normalised with respect to α_2, are given in Table 7, where the superscript *up*, *down* and *tot* denote that CTEs are computed for the upper arm of the specimen, the lower one, or the complete laminate, respectively. From a qualitative point of view, one can immediately observe that sequence QT is the only one showing a behaviour that effectively mimics that of the *UD* sequence:

1. bending CTEs are identically null for all portions of the specimen. This follows immediately from Eqs. (A.7) and (A.10), when $\mathbf{B} = \mathbf{0}$ and $\mathbf{V} = \mathbf{0}$;
2. in-plane shear CTE (third component of $\boldsymbol{\alpha}_\epsilon$) is identically null for all the portions of the specimens. Indeed, each arms and the entire portion of a FUMD laminate have orthotropic matrix $\mathbf{A}$ (i.e. $\mathrm{A}_{16} = \mathrm{A}_{26} = 0$) and identically null third component of vector $\mathbf{U}$, as it can be readily verified from Eqs. (4) and (5). As a consequence, and by having also $\mathbf{B} = \mathbf{0}$, it follows from (A.6) that matrix $\mathbf{a}$ is still an orthotropic one. Hence, from Eq. (A.10), the third component of $\boldsymbol{\alpha}_\epsilon$ is identically null;
3. no mismatches of CTEs among the different parts of the specimen exist.

Hence, from a thermo-mechanical point of view and in the framework of CLPT, FUMD sequences effectively behave as a purely UD one, and sequence QT is the only one achieving this result among the sequences compared.

[Table 7 about here.]

References

[1] A. C. Garg, Delamination-a damage mode in composite structures, Engineering Fracture Mechanics 29 (5) (1988) 557–584. doi:10.1016/0013-7944(88)90181-6.

[2] Delamination-dominated failures in polymer composites, in: E. S. Greenhalgh (Ed.), Failure Analysis and Fractography of Polymer Composites, Woodhead Publishing Series in Composites Science and Engineering, Woodhead Publishing, 2009, pp. 164 – 237. doi:https://doi.org/10.1533/9781845696818.164.
URL http://www.sciencedirect.com/science/article/pii/B9781845692179500044

[3] M. Heidari-Rarani, M. Shokrieh, P. Camanho, Finite element modeling of mode i delamination growth in laminated dcb specimens with r-curve effects, Composites Part B: Engineering 45 (1) (2013) 897–903.

[4] J. Babu, T. Sunny, N. A. Paul, K. P. Mohan, J. Philip, J. P. Davim, Assessment of delamination in composite materials: A review, Proceedings of the Institution of Mechanical Engineers, Part B: Journal of Engineering Manufacture 230 (11) (2016) 1990–2003. doi:10.1177/0954405415619343.

[5] I. Raju, T. O'Brien, Fracture mechanics concepts, stress fields, strain energy release rates, delamination initiation and growth criteria, in: S. Sridharan (Ed.), Delamination Behaviour of Composites, Woodhead Publishing Series in Composites Science and Engineering, Woodhead Publishing, 2008, pp. 3 – 27. doi:10.1533/9781845694821.1.3.
URL http://www.sciencedirect.com/science/article/pii/B9781845692445500018

[6] A. A. Griffith, The Phenomena o f Rupture and Flow in Solids, Philosophical Transactions of the Royal Society of London. Series A, Containing

Papers of a Mathematical or Physical Character. 221 (582-593) (1921) 163–198. doi:https://doi.org/10.1098/rsta.1921.0006.
URL https://royalsocietypublishing.org/doi/abs/10.1098/rsta.1921.0006

[7] G. R. Irwin, Onset of fast crack propagation in high strength steel and aluminum alloys, Tech. rep., NAVAL RESEARCH LAB WASHINGTON DC (1956).

[8] G. R. Irwin, Fracture, Springer Berlin Heidelberg, Berlin, Heidelberg, 1958, pp. 551–590. doi:10.1007/978-3-642-45887-3_5.
URL https://doi.org/10.1007/978-3-642-45887-3_5

[9] E. J. Barbero, Finite element analysis of composite materials using Abaqus.

[10] T. K. O'Brien, Interlaminar fracture toughness: The long and winding road to standardization, Composites Part B: Engineering 29 (1) (1998) 57–62. doi:10.1016/S1359-8368(97)00013-9.

[11] ASTM-D5528-13, Standard Test Method for Mode I Interlaminar Fracture Toughness of Unidirectional Fiber-Reinforced Polymer Matrix Composites, ASTM Interntional, West Conshohocken, PA (2013).
URL www.astm.org

[12] A. D7905/7905M-14, Standard Test Method for Determination of the Mode II Interlaminar Fracture Toughness of Unidirectional Fiber-Reinforced Polymer, ASTM Interntional, West Conshohocken, PA (2014).
URL www.astm.org

[13] ASTM 6671/D 6671M – 06, Standard Test Method for Mixed Mode I-Mode II Interlaminar Fracture Toughness of Unidirectional Fiber Reinforced Polymer Matrix Composites, ASTM International, West Conshohocken, PA (2013).
URL www.astm.org

[14] S. M. Lee, An Edge Crack Torsion Method for Mode III Delamination Fracture Testing, Journal of Composites Technology & Research, JCTRER 15 (3) (1993) 193–201. doi:10.1520/CTR10369J.

[15] J. Andersons, M. König, Dependence of fracture toughness of composite laminates on interface ply orientations and delamination growth direction, Composites Science and Technology 64 (13-14) (2004) 2139–2152. doi:10.1016/j.compscitech.2004.03.007.

[16] M. Nikbakht, J. Yousefi, H. Hosseini-Toudeshky, G. Minak, Delamination evaluation of composite laminates with different interface fiber orientations using acoustic emission features and micro visualization, Composites Part B: Engineering 113 (2017) 185–196. doi:10.1016/j.compositesb.2016.11.047.

[17] J. Tao, C. T. Sun, Influence of ply orientation on delamination in composite laminates, Journal of Composite Materials 32 (21) (1998) 1933–1947. arXiv:https://doi.org/10.1177/002199839803202103, doi:10.1177/002199839803202103.
URL https://doi.org/10.1177/002199839803202103

[18] A. A. Benyahia, A. Laksimi, N. Ouali, Z. Azari, Mechanical behavior and optimization of multidirectional laminate specimens under delamination by bending, Strength of Materials 38 (6) (2006) 613–623. doi:10.1007/s11223-006-0083-9.

[19] T. A. Sebaey, N. Blanco, C. S. Lopes, J. Costa, Numerical investigation to prevent crack jumping in Double Cantilever Beam tests of multidirectional composite laminates, Composites Science and Technology 71 (13) (2011) 1587–1592. doi:10.1016/j.compscitech.2011.07.002.
URL http://dx.doi.org/10.1016/j.compscitech.2011.07.002

[20] T. A. Sebaey, N. Blanco, J. Costa, C. S. Lopes, Characterization of crack propagation in mode I delamination of multidirectional CFRP laminates,

Composites Science and Technology 72 (11) (2012) 1251–1256. doi:10.1016/j.compscitech.2012.04.011.
URL http://dx.doi.org/10.1016/j.compscitech.2012.04.011

[21] J. A. Nairn, Fracture Mechanics of Composites With Residual Thermal Stresses, Journal of Applied Mechanics 64 (4) (1997) 804. doi:10.1115/1.2788985.

[22] J. A. Nairn, Energy release rate analysis for adhesive and laminate double cantilever beam specimens emphasizing the effect of residual stresses, International Journal of Adhesion and Adhesives 20 (1) (2000) 59–70. doi:10.1016/S0143-7496(99)00016-0.

[23] J. A. Nairn, On the calculation of energy release rates for cracked laminates with residual stresses, International Journal of Fracture 139 (2) (2006) 267–293. doi:10.1007/s10704-006-0044-0.

[24] T. Yokozeki, T. Ogasawara, T. Aoki, Correction method for evaluation of interfacial fracture toughness of DCB, ENF and MMB specimens with residual thermal stresses, Composites Science and Technology 68 (3-4) (2008) 760–767. doi:10.1016/j.compscitech.2007.08.025.

[25] A. B. De Morais, M. F. De Moura, J. P. Gonçalves, P. P. Camanho, Analysis of crack propagation in double cantilever beam tests of multidirectional laminates, Mechanics of Materials 35 (7) (2003) 641–652. doi:10.1016/S0167-6636(02)00289-2.

[26] R. Krueger, Virtual crack closure technique: History, approach, and applications, Applied Mechanics Reviews 57 (2) (2004) 109. doi:10.1115/1.1595677.
URL http://appliedmechanicsreviews.asmedigitalcollection.asme.org/article.aspx?articleid=1397949

[27] R. Krueger, K. N. Shivakumar, I. S. Raju, Fracture Mechanics Analyses for Interface Crack Problems - A Review, 54th

AIAA/ASME/ASCE/AHS/ASC Structures, Structural Dynamics, and Materials Conference (September 2015) (2013). doi:10.2514/6.2013-1476.
URL http://arc.aiaa.org/doi/10.2514/6.2013-1476

[28] B. D. Davidson, R. A. Schapery, Effect of Finite Width on Deflection and Energy Release Rate of an Orthotropic Double Cantilever Specimen, Journal of Composite Materials 22 (7) (1988) 640–656. doi:10.1177/002199838802200704.

[29] B. D. Davidson, An Analytical Investigation of Delamination Front Curvature in Double Cantilever Beam Specimens, Journal of Composite Materials 24 (11) (1990) 1124–1137. doi:10.1177/002199839002401101.

[30] C. T. Sun, S. Zheng, Delamination characteristics of double-cantilever beam and end-notched flexure composite specimens, Composites Science and Technology 56 (4) (1996) 451–459. doi:10.1016/0266-3538(96)00001-2.
URL http://www.sciencedirect.com/science/article/pii/0266353896000012

[31] B. D. Davidson, R. Kruger, M. Konig, Effects of Stacking Sequence on Energy Release Rate Distributions in Multidirectional DCB and ENF Specimens, Engineering Fracture Mechanics 55 (4) (1996) 557–569. doi:10.1016/S0013-7944(96)00037-9.

[32] S. Samborski, Numerical analysis of the DCB test configuration applicability to mechanically coupled Fiber Reinforced Laminated Composite beams, Composite Structures 152 (2016) 477–487. doi:10.1016/j.compstruct.2016.05.060.
URL http://dx.doi.org/10.1016/j.compstruct.2016.05.060

[33] B. D. Davidson, S. J. Gharibian, L. Yu, Evaluation of energy release rate-based approaches for predicting delamination growth in laminated composites, International Journal of Fracture 105 (4) (2000) 343–365. doi:10.1023/A:1007647226760.

[34] B. D. Davidson, R. D. Bialaszewski, S. S. Sainath, A non-classical, energy release rate based approach for predicting delamination growth in graphite reinforced laminated polymeric composites, Composites Science and Technology 66 (10) (2006) 1479–1496. doi:10.1016/j.compscitech.2004.10.031.

[35] P. Vannucci, G. Verchery, A special class of uncoupled and quasi-homogeneous laminates, Composites Science and Technology 61 (10) (2001) 1465–1473. doi:10.1016/S0266-3538(01)00039-2.

[36] M. S. Mohamed Rehan, J. Rousseau, X. J. Gong, L. Guillaumat, J. S. Ali, Effects of fiber orientation of adjacent plies on the mode I crack propagation in a carbon-epoxy laminates, Procedia Engineering 10 (2011) 3179–3184. doi:10.1016/j.proeng.2011.04.525.
URL http://dx.doi.org/10.1016/j.proeng.2011.04.525

[37] M. S. Bin Mohamed Rehan, J. Rousseau, S. Fontaine, X. J. Gong, Experimental study of the influence of ply orientation on DCB mode-I delamination behavior by using multidirectional fully isotropic carbon/epoxy laminates, Composite Structures 161 (2017) 1–7. doi:10.1016/j.compstruct.2016.11.036.
URL http://dx.doi.org/10.1016/j.compstruct.2016.11.036

[38] X. J. Gong, A. Hurez, G. Verchery, On the determination of delamination toughness by using multidirectional DCB specimens, Polymer Testing 29 (6) (2010) 658–666. doi:10.1016/j.polymertesting.2010.04.007.
URL http://dx.doi.org/10.1016/j.polymertesting.2010.04.007

[39] T. Garulli, A. Catapano, M. Montemurro, J. Jumel, D. Fanteria, Quasi-trivial stacking sequences for the design of thick laminates, Composite Structures 200 (2018) 614–623. doi:10.1016/j.compstruct.2018.05.120.

[40] T. Garulli, A. Catapano, M. Montemurro, J. Jumel, D. Fanteria, Quasi-trivial solutions for uncoupled, homogeneous and quasi-homogeneous lam-

inates with high number of plies, in: R. Owen, de Borst, Pearce (Eds.), ECCM VI, International Center for Numerical Methods in Engineering (CIMNE), pp. 255–265.

[41] E. F. Rybicki, M. F. Kanninen, A finite element calculation of stress intensity factors by a modified crack closure integral, Engineering Fracture Mechanics 9 (4) (1977) 931–938. doi:10.1016/0013-7944(77)90013-3.

[42] K. N. Shivakumar, P. W. Tan, J. C. Newman, A virtual crack-closure technique for calculating stress intensity factors for cracked three dimensional bodies, International Journal of Fracture 36 (3) (1988) R43–R50.

[43] M. L. WILLIAMS, The Streses Around Faults In Dissimilar Media, Bulletin of the Seismological Society of America 49 (2) (1959) 199–204.

[44] I. S. Raju, J. H. Crews, M. A. Aminpour, Convergence of strain energy release rate components for Edge-Delaminated composite laminates, Engineering Fracture Mechanics 30 (3) (1988) 383–396. doi:10.1016/0013-7944(88)90196-8.

[45] P. S. Valvo, A revised virtual crack closure technique for physically consistent fracture mode partitioning, International Journal of Fracture 173 (1) (2012) 1–20. doi:10.1007/s10704-011-9658-y.

[46] P. S. Valvo, A Physically Consistent Virtual Crack Closure Technique for I/II/III Mixed-mode Fracture Problems, Procedia Materials Science 3 (September) (2014) 1983–1987. doi:10.1016/j.mspro.2014.06.319. URL http://linkinghub.elsevier.com/retrieve/pii/S2211812814003204

[47] P. S. Valvo, A further step towards a physically consistent virtual crack closure technique, International Journal of Fracture 192 (2) (2015) 235–244. doi:10.1007/s10704-015-0007-4.

[48] M. M. Shokrieh, M. Heidari-Rarani, S. Rahimi, Influence of curved delamination front on toughness of multidirectional DCB specimens, Composite

Structures 94 (4) (2012) 1359–1365. doi:10.1016/j.compstruct.2011.11.035.

URL http://dx.doi.org/10.1016/j.compstruct.2011.11.035

[49] P. Vannucci, Anisotropic Elasticity, Vol. 85, 2018. doi:10.1007/978-981-10-5439-6.

[50] J. Schön, T. Nyman, A. Blom, H. Ansell, Numerical and experimental investigation of a composite ENF-specimen, Engineering Fracture Mechanics 65 (4) (2000) 405–433. doi:10.1016/S0013-7944(99)00137-X.

[51] Z. H. Xie, X. Li, J. Zhao, J. Hao, Y. P. Sun, X. D. Sui, Study on the mode i interlaminar fracture toughness of multi-directional composite laminates, in: Advanced Measurement and Test III, Vol. 718 of Advanced Materials Research, Trans Tech Publications, 2013, pp. 186–190. doi:10.4028/www.scientific.net/AMR.718-720.186.

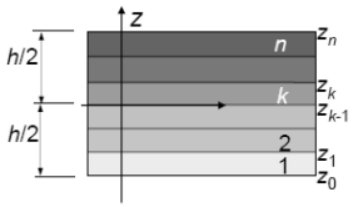

Figure 1: Laminate stack parameters and notation.

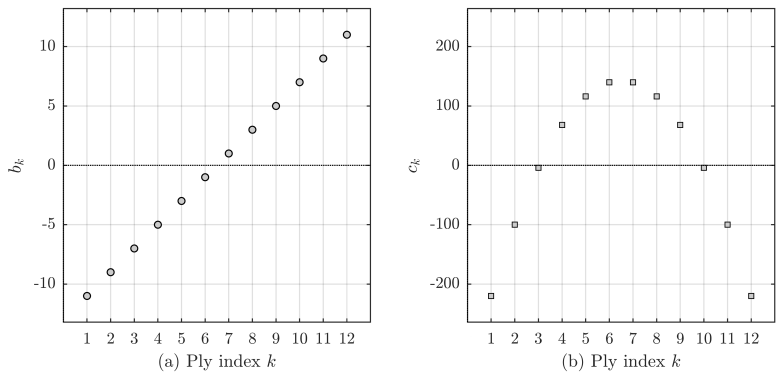

Figure 2: Trend of coefficient b_k, (a), and c_k, (b), with respect to the ply position index k.

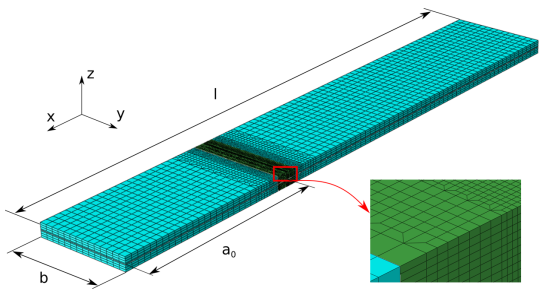

Figure 3: DCB finite element model and detail of the central refined region.

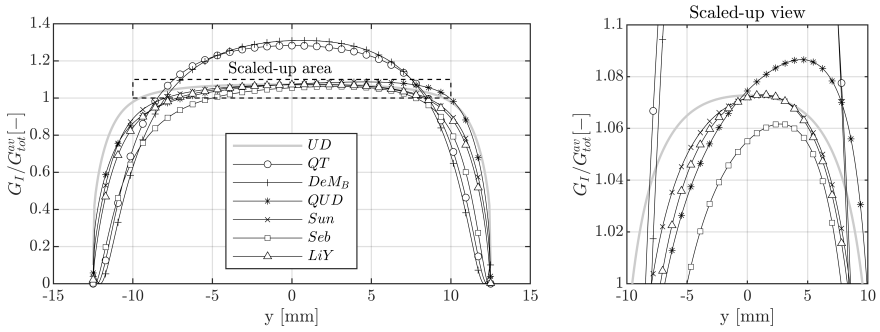

Figure 4: Normalised mode I ERR distribution along crack front, found using standard VCCT.

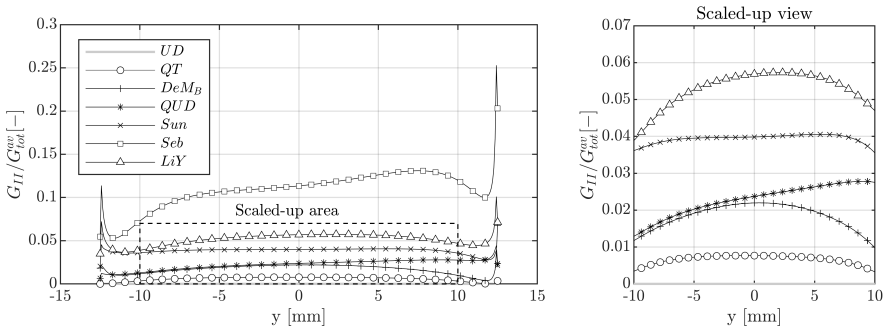

Figure 5: Normalised mode II ERR distribution along crack front, found using standard VCCT.

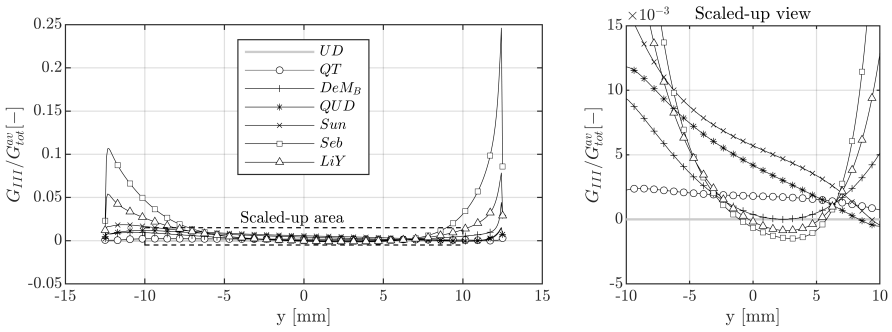

Figure 6: Normalised mode III ERR distribution along crack front, found using standard VCCT.

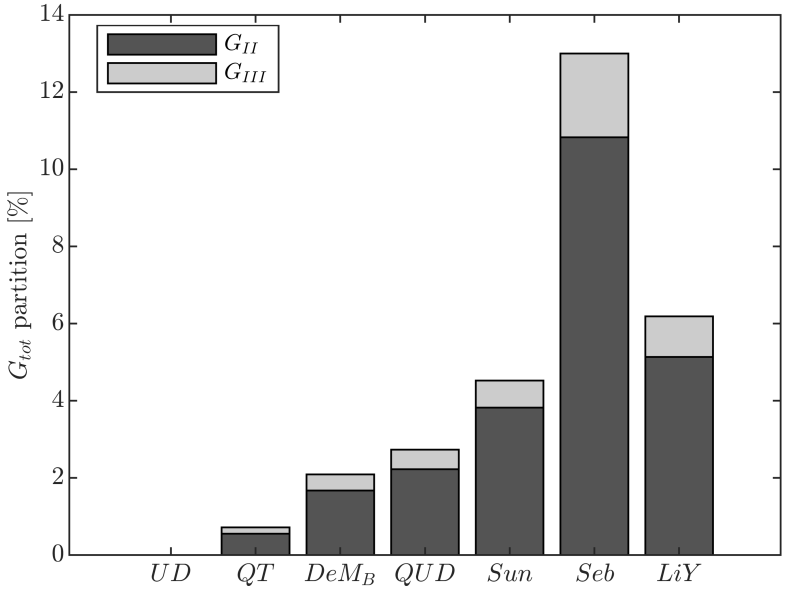

Figure 7: Percent overall modes II and II ERR contributes, found using standard VCCT.

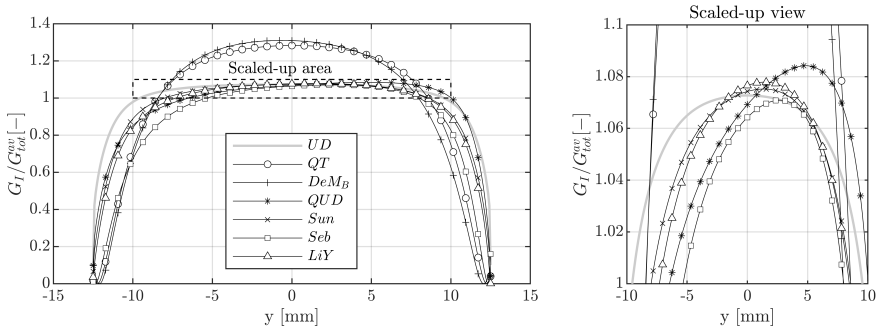

Figure 8: Normalised mode I ERR distribution along crack front, found using revised VCCT.

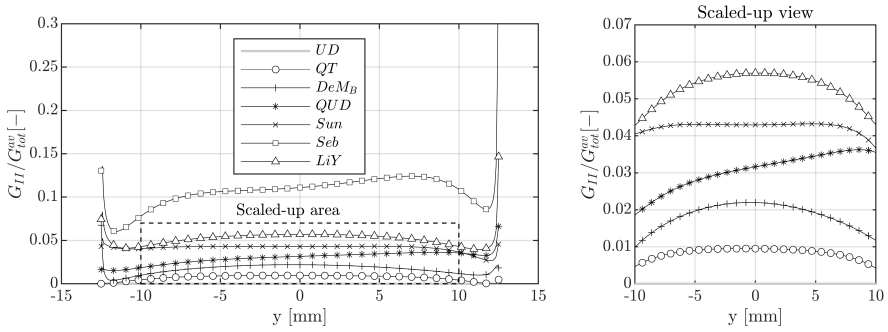

Figure 9: Normalised mode II ERR distribution along crack front, found using revised VCCT.

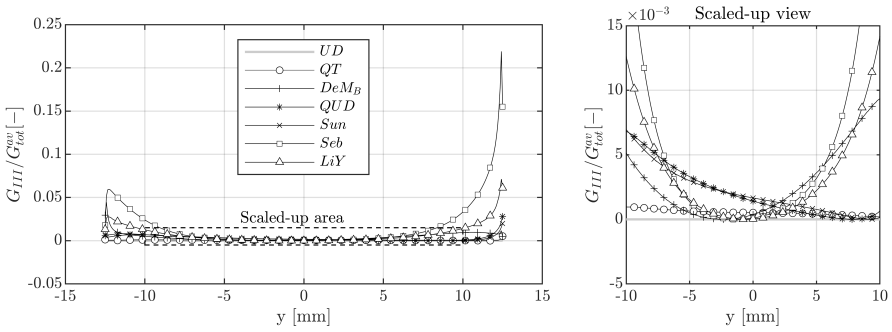

Figure 10: Normalised mode III ERR distribution along crack front, found using revised VCCT.

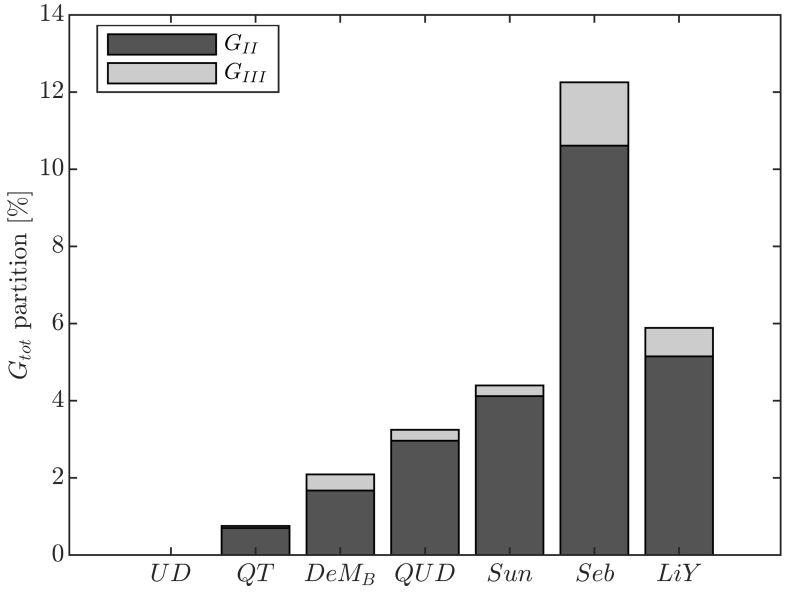

Figure 11: Percent overall modes II and III ERR contributes, found using revised VCCT.

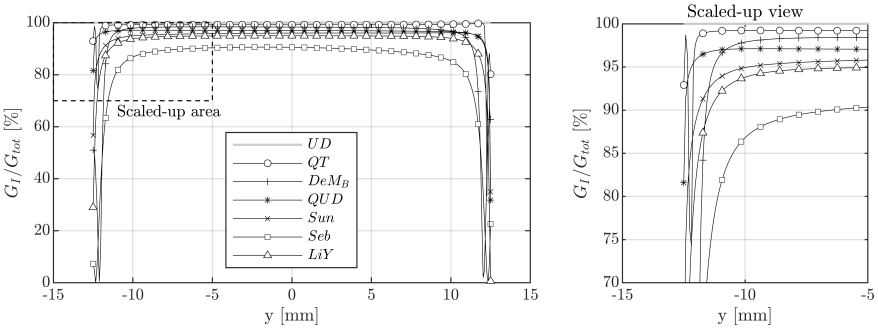

Figure 12: Local percent contribution of mode I ERR along crack front.

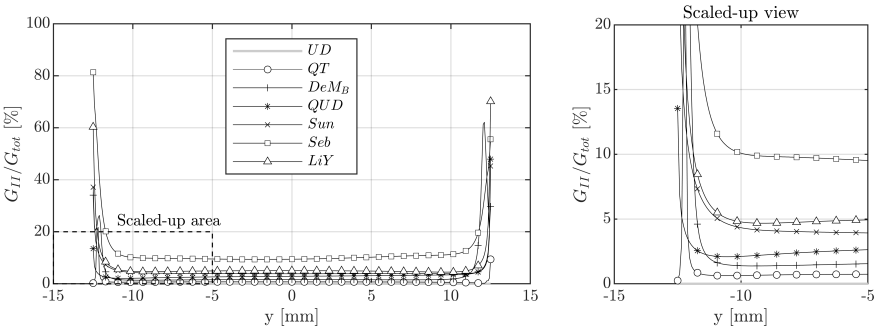

Figure 13: Local percent contribution of mode II ERR along crack front.

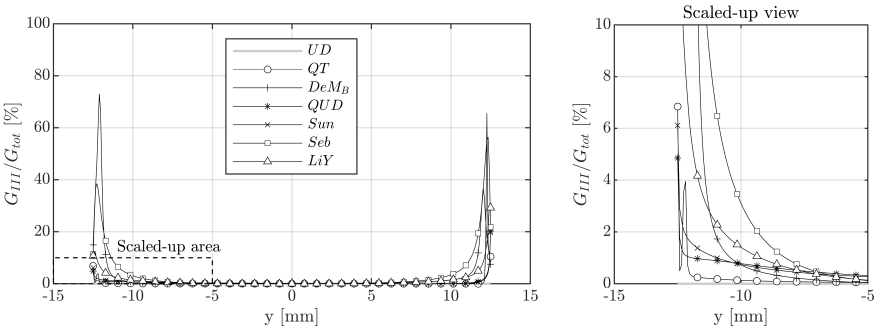

Figure 14: Local percent contribution of mode III ERR along crack front.

Label	Stacking sequence	$D_{11}^{*,down}/D_{11}^{*,up}/D_{11}^{*}$ [GPa]
UD [11]	$[0]_{28}$	113,8 / 113,8 / 113,8
QT	[0/45/-45/-45/0/45/0/0/45/0/-45/-45/45/0// 45/0/-45/0/0/-45/-45/45/45/0/0/45/0/-45]	69,46 / 69,46 / 69,46
DeM_B [25]	$[(0/\mp 45)_4//(0/\mp 45)_4]$	62,79 / 62,79 / 62,25
QUD [50]	$[0_{14}//45/0_{13}]$	113,8 / 99,41 / 113,8
Sun [30]	$[0_{14}//45/0_{12}/-45]$	113,8 / 85,06 / 106,0
Seb [20]	$[0_{12}//45/-45/0_8/-45/45]$	113,8 / 59,20 / 97,26
LiY [51]	$[0_{14}//45/-45/0_{12}]$	113,8 / 89,13 / 113,7

Table 1: Stacking sequences analysed and associated labels. The double slash indicates mid-plane (delamination) interface.

	UD	QT	DeM_B	QUD	Sun	Seb_{S4}	LiY
D_c^{down}	0.0094	0.18802	0.24096	0.0094	0.0094	0.0094	0.0094
B_t^{down}	0	0	0.01143	0	0	0	0
$\mathbf{B}^*_{down} = \mathbf{0}$	✓	✓	X	✓	✓	✓	✓
$\mathbf{C}_{down} = \mathbf{0}$	✓	✓	X	✓	✓	✓	✓

Table 2: Elastic properties of the lower arm sequences.

	UD	QT	DeM_B	QUD	Sun	Seb_{S4}	LiY
$D^{up}_{\mathcal{C}}$	0.0094	0.18802	0.24096	0.04374	0.09826	0.27458	0.08056
B^{up}_t	0	0	0.01143	0.0481	0	0.0606	0.01521
$\mathbf{B}^*_{up} = \mathbf{0}$	✓	✓	X	X	X	✓	X
$\mathbf{C}_{up} = \mathbf{0}$	✓	✓	X	X	X	X	X

Table 3: Elastic properties of the upper arm sequences.

	UD	QT	DeM_B	QUD	Sun	Seb_{S4}	LiY
D_c	0.009404	0.188022	0.245745	0.009428	0.025451	0.050592	0.009593
B_t	0	0	0.002881	4.1e-05	0.024238	0.004611	0.000248
$\mathbf{B}^* = \mathbf{0}$	✓	✓	X	X	X	X	X
$\mathbf{C} = \mathbf{0}$	✓	✓	X	X	X	X	X
$\mathbf{A}^*_{up} = \mathbf{A}^*_{down}$	✓	✓	✓	X	X	X	X
$\mathbf{B}^*_{up} = \mathbf{B}^*_{down}$	✓	✓	✓	X	X	✓	X
$\mathbf{C}_{up} = \mathbf{C}_{down}$	✓	✓	✓	X	X	X	X
$\mathbf{D}^*_{up} = \mathbf{D}^*_{down}$	✓	✓	✓	X	X	X	X

Table 4: Elastic properties of entire sequences.

E_{11} [Gpa]	E_{22} [Gpa]	G_{12} [Gpa]	ν_{12}	ν_{23}
112.7	10.35	3.5	0.32	0.42

Table 5: Constitutive lamina properties

	UD	QT	DeM_B	QUD	Sun	Seb_{S4}	LiY
G_2 %	0	0.7	1.68	2.96	4.12	10.61	5.15
G_3 %	0	0.05	0.41	0.28	0.28	1.64	0.74
β	0.0727	0.2925	0.3383	0.1208	0.1248	0.2217	0.1459
γ	0	0.0147	0.0406	0.092	0.0215	0.1006	0.037

Table 6: Representative parameters of ERR distributions.

	UD	QT	DeM_B	QUD	Sun	Seb_{S4}	LiY	
α_ϵ^{up}	-0.00222	0.0222	0.0430	0.000413	0.00283	0.00154	0.00157	[-]
	1	0.609	0.5730	0.960	0.927	0.710	0.892	
	0	0	0.00487	-0.0799	0	0	0.0156	
α_χ^{up}	0	0	0.0469	-0.00841	0	0	-0.0113	$[\frac{1}{mm}]$
	0	0	-0.0881	0.1265	0	0	0.317	
	0	0	-0.0526	0.253	0.451	0	0.0150	
α_ϵ^{down}	-0.00222	0.0222	0.0430	-0.00222	-0.00222	-0.00222	-0.00222	[-]
	1	0.609	0.573	1	1	1	1	
	0	0	0.00487	0	0	0	0	
α_χ^{down}	0	0	0.0469	0	0	0	0	$[\frac{1}{mm}]$
	0	0	-0.0881	0	0	0	0	
	0	0	-0.0526	0	0	0	0	
α_ϵ^{tot}	-0.00222	0.0222	0.0393	-0.00271	-0.00251	-0.00130	-0.00387	[-]
	1	0.609	0.573	0.957	0.925	0.842	0.905	
	0	0	0.00119	-0.110	-0.0477	-0.00330	-0.000906	
α_χ^{tot}	0	0	0.0115	-2.95e-05	0.000584	0.00291	-0.000201	$[\frac{1}{mm}]$
	0	0	-0.0217	-0.00260	-0.0521	-0.131	-0.0116	
	0	0	-0.0128	-0.00672	0.110	0.00798	0.0151	

Table 7: Equivalent laminates CTEs of the sequences compared, normalised by α_2, and for both arms and the entire laminate.